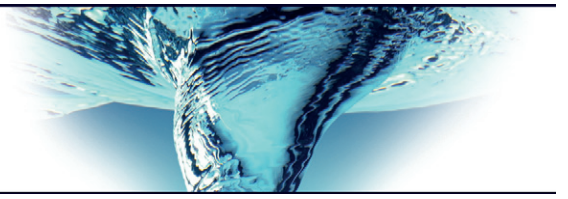
J. Fluid Mech. (2014), *vol.* 758, R2, doi:10.1017/jfm.2014.562



JFM RAPIDS
journals.cambridge.org/rapids

Transverse dam-break waves

S. Karimpour Ghannadi[1] **and Vincent H. Chu**[1,†]

[1]Department of Civil Engineering and Applied Mechanics, McGill University, Montreal, QC, H3A 0C3, Canada

(Received 25 July 2014; revised 16 September 2014; accepted 23 September 2014; first published online 7 October 2014)

Numerical simulations of the transverse dam-break waves (TDWs) produced by the sudden removal of a gate on the side of a waterway are conducted based on the shallow-water equations to find solutions to a family of water-diversion problems. The Froude numbers in the main flow identify the members of the family. The depth and discharge profiles are analysed in terms of Ritter's similarity variable. For subcritical main flow, the waves are comprised of a supercritical flow expansion followed by a subcritical outflow. For supercritical main flow, on the other hand, the waves are analogous to the Prandtl–Meyer expansion in gas dynamics. The diversion flow rate of two-dimensional TDWs on a flat bed is 55 % greater than the one-dimensional flow rate of Ritter in the limiting case of zero main flow, and approaches the rate of Ritter in the other limit when the value of the Froude number in the main flow approaches infinity. The diversion flow rate over a weir is generally higher than the rate over a flat bed depending on the Froude number of the main flow. These numerical simulation results are consistent with laboratory observations.

Key words: computational methods, geophysical and geological flows, waves/free-surface flows

1. Introduction

The diversion of water from the main flow to the side is a ubiquitous occurrence in natural and man-made waterways. It has found applications in irrigation, in flood control and in the municipal and industrial conveyance of water. The engineering design for diversion structures has been dependent on empirical formulae and more recently on numerical simulations. For the diversion flow over a side weir, Subramanya & Awasthy (1972) proposed semi-empirical discharge formulae based on laboratory experimental data. Mizumura, Yamasaka & Adachi (2003), on the other hand, acquired experimental data and formulated the supercritical flow diversion on a flat bed using the analogy between open-channel hydraulics and gas dynamics. Ritter (1892) introduced a similarity variable in his solution to the one-dimensional (1D) dam-break wave problem.

† Email address for correspondence: vincent.chu@mcgill.ca

© Cambridge University Press 2014

https://doi.org/10.1017/jfm.2014.562 Published online by Cambridge University Press

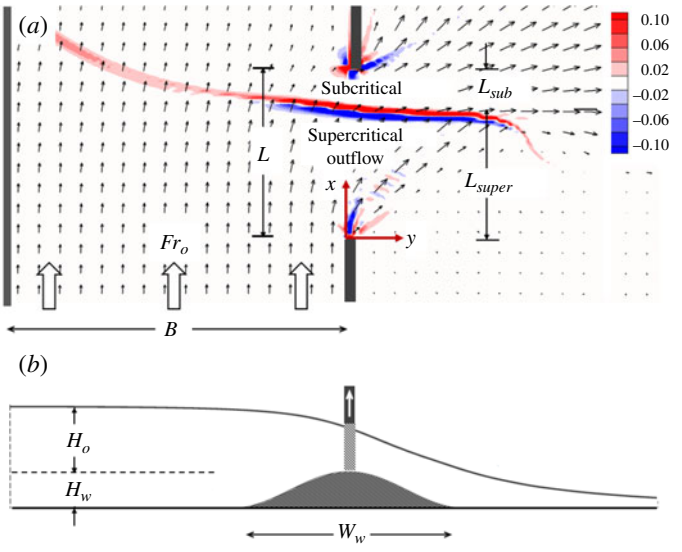


FIGURE 1. TDWs over a length of L on the side of the open-channel main flow. (a) The arrows show the velocity vector ($\boldsymbol{u}$, $\boldsymbol{v}$). The sharp change in dilation ($\partial \boldsymbol{u}/\partial x + \partial \boldsymbol{v}/\partial y$) from blue to red marks the hydraulic jump as the outflow changes from supercritical to subcritical. The flow pattern shown is obtained from a simulation for the main-flow Froude number $Fr_o = 0.63$. The length along the opening of the supercritical outflow upstream of the jump is L_{super}. The length of the subcritical outflow is L_{sub}. (b) Cross-sectional profile of water depth and bottom elevation over a weir of height H_w and width W_w.

This paper describes numerical simulations conducted to study the diversion of water from the main flow. The results are analysed as a family of transverse dam-break waves (TDWs) defined by the Froude number of the main flow. When correctly implemented, numerical simulation can be accurate and can provide in-depth understanding that is equal to analytical methods. The present simulation complements a number of recent works on related dam-break waves, by Hogg & Pritchard (2004), Vazquez, Kesserwani & Riviere (2008), Ghostine *et al.* (2013) and Mahmodinia, Javan & Eghbalzadeh (2014).

Figure 1 delineates the two-dimensional (2D) problem of the TDWs produced by the sudden removal of a gate on the side of a waterway. The height of the weir on the side is H_w. The undisturbed water level above the crest of the weir is H_o. The velocity and depth of the undisturbed main flow, U and H, define the Froude number of the main flow, $Fr_o = U/\sqrt{gH}$, where g is gravity. The lateral outflow through the gate opening can be subcritical, supercritical or a combination of both.

This paper has six sections including this introductory section. Section 2 explains the numerical simulations and the implementation of the shock-capturing scheme for the simulations. The results for the family of TDWs are related on the one hand to the analogous problem of the Prandtl–Meyer expansion in gas dynamics (the Prandtl–Meyer expansion is a supersonic expansion wave of compressible gas along an outwardly bent wall (see, e.g., Liepmann & Roshko 2013)) and on the other hand to the classical 1D dam-break waves of Ritter (1892). Sections 3 and 4 present the simulation results for the transient and steady-state development of the waves on a flat bed. In § 5, the simulations are repeated for the TDWs over a weir. The simulations

https://doi.org/10.1017/jfm.2014.562 Published online by Cambridge University Press

are compared with laboratory measurements. A summary and conclusion are given in § 6.

2. Numerical simulation

The simulations for the TDWs are based on numerical solutions of shallow-water equations:

$$\frac{\partial h}{\partial t}+\frac{\partial q_x}{\partial x}+\frac{\partial q_y}{\partial y}=0, \tag{2.1}$$

$$\frac{\partial q_x}{\partial t}+\frac{\partial\,(\boldsymbol{u}q_x)}{\partial x}+\frac{\partial\,(\boldsymbol{v}q_x)}{\partial y}=-\frac{1}{2}gh\frac{\partial(h+z_o)}{\partial x}, \tag{2.2}$$

$$\frac{\partial q_y}{\partial t}+\frac{\partial\,(\boldsymbol{u}q_y)}{\partial x}+\frac{\partial\,(\boldsymbol{v}q_y)}{\partial y}=-\frac{1}{2}gh\frac{\partial(h+z_o)}{\partial y}, \tag{2.3}$$

where h = flow depth, z_o = channel-bottom elevation, $(\boldsymbol{u}, \boldsymbol{v})$ = velocity components, $(q_x, q_y)=(\boldsymbol{u}h, \boldsymbol{v}h)$ = discharge components in the x and y directions, respectively. For flow on a flat bed ($z_o=0$), these shallow-water equations are identical to 2D gas-dynamic equations when the specific heat ratio is 2; see, e.g., Liggett (1994).

An improved version of the numerical scheme by Pinilla *et al.* (2010) is used for the numerical simulations. A staggered grid defines the nodal values for h, q_x and q_y in the computational domain. The MINMOD flux limiter determines the momentum fluxes on the faces of the finite volume. This maintains the stability of the computation by controlling the spurious numerical oscillations initiated across the hydraulic jump. A fourth-order Runge–Kutta scheme is employed for integration in time. The MINMOD flux limiter is known to be somewhat diffusive; see, e.g., Chu & Gao (2013). It is, however, acceptable for simulations of depth and velocity profiles that are not sensitive to false diffusion. Other flux limiters mentioned in Sweby (1984) have been used in this study but have produced no significant difference in results.

The numerical simulation starts with a given velocity U and depth H in the main channel. Removal of the gate on the side of length L produces the TDWs. For the flow profiles presented in this paper, the length of the opening on the side is $L=25$ m and the water depth is $H_o=1$ m. The width selected for the main channel is $B=8L$ for subcritical main flow ($Fr_o<1$). For supercritical main flow ($Fr_o>1$), the width is $B=8L/Fr_o$. These widths are selected to avoid the effect of wave reflection. There are 100 nodes over the length of the opening. The grid sizes therefore are $\Delta x=\Delta y=L/100$. Grid-refinement study has shown that this grid-size selection has a better than one per cent accuracy on the discharge coefficient.

3. Transient development toward the steady state

Figures 2(*a*,*b*) show the transient development of the TDWs toward the steady state for main-flow Froude numbers of $Fr_o=0.03$ and 0.63, respectively. There are three subsets of figures for each Fr_o. The top left in each subset contains the depth h-profiles obtained on the centre plane, where $x=0.5L$ for time $t/t_s=0.25$, 0.75, 1.5 and 3.0. The bottom left are the lateral outflow q_y-profiles on the centre plane for the same period of time. The four images on the right show the contours of the local Froude number $Fr=\sqrt{\boldsymbol{u}^2+\boldsymbol{v}^2}/\sqrt{gh}$ on the x–y plane. The local Froude number Fr delineates the evolution of the flow due to the waves over a period of $t/t_s=0.25$, 0.5, 1.0 to 1.5. The area of supercritical flow with $Fr>1$ is marked in red. The

https://doi.org/10.1017/jfm.2014.562 Published online by Cambridge University Press

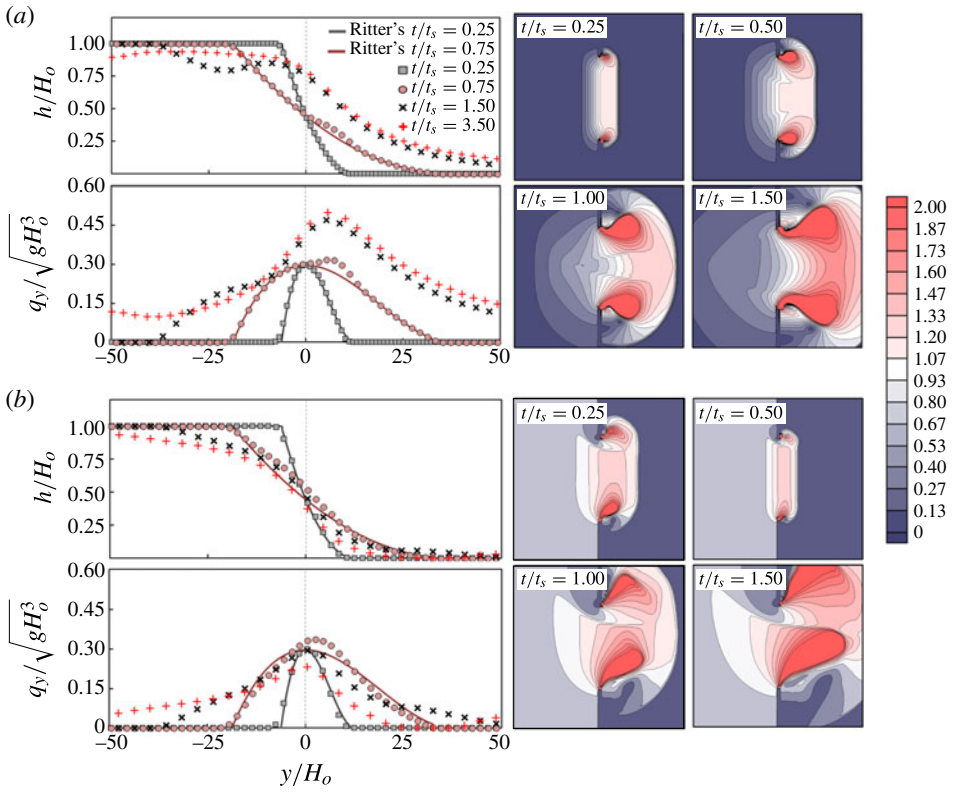


FIGURE 2. Transient development of TDWs on a flat bed for $Fr_o =$ (*a*) 0.03 and (*b*) 0.63 over the period from time $t/t_s = 0.25$ to 3.00. The depth (top left) and lateral discharge (bottom left) profiles are obtained at the centre of the opening where $x = L/2$. The contour lines in the images (right) define the local Froude number $Fr = \sqrt{\boldsymbol{u}^2 + \boldsymbol{v}^2}/\sqrt{gh}$. The red colour marks the region of the supercritical flow ($Fr > 1$).

subcritical flow with $Fr < 1$ is marked in grey. The critical-flow section where $Fr = 1$ is defined by the contour line between the red and the grey. The flow pattern changes rapidly with time. The time scale for the transient development is the communication time $t_s = L/\sqrt{gH_o}$, which is approximately the time needed for the wave of speed $c = \sqrt{gH_o}$ to travel from one end of the gate opening to the other end.

Immediately after the removal of the gate, the critical-flow contour is located at the gate where $y = 0$. The contour moves forward with time in the direction of the flow. In the case of a small main-flow Froude number of $Fr_o = 0.03$, as shown in figure 2(*a*), the outflow at the gate opening is subcritical as the flow approaches the steady state. At a higher main-flow Froude number of $Fr_o = 0.63$, as shown in figure 2(*b*), the outflow at the leading edge is a supercritical flow expansion followed by a subcritical outflow. The depth and velocity change rapidly across the jump from supercritical to subcritical outflow.

3.1. *The 1D dam-break waves of Ritter*

The initial TDW profiles follow closely the one-dimensional (1D) dam-break wave profiles of Ritter (1892), which are the solid lines in figure 2. These profiles remain

https://doi.org/10.1017/jfm.2014.562 Published online by Cambridge University Press

close to the 1D solution of Ritter as long as the waves from the opposite edges of the opening have not reached the cross-section. The later development of the 2D TDWs can also be described by Ritter's similarity variable. A brief summary of the 1D solution of Ritter is therefore given in this subsection for comparison with the 2D simulation results in later sections.

The 1D wave does not have a steady state. The flow through the critical-flow section nevertheless stays constant throughout the development of the waves. The removal of the dam in the 1D channel produces a positive wave and a negative wave. The front of the positive wave advances with a velocity equal to $\boldsymbol{v} = 2\sqrt{gH_o}$. The recessing edge has a negative velocity equal to $\boldsymbol{v} = -\sqrt{gH_o}$. The similarity variable of Ritter is

$$R = \frac{y}{t\sqrt{gH_o}}, \tag{3.1}$$

which unifies the space y and time t through the wave speed $\sqrt{gH_o}$. The profiles for the depth and discharge of the 1D wave expressed in terms of Ritter's similarity variable are

$$\frac{h}{H_o} = \frac{1}{9}(2-R)^2, \quad \frac{q_y}{\sqrt{gH_o^3}} = \frac{2}{27}(1+R)(2-R)^2 \quad \text{for } -1 < R < 2. \tag{3.2a,b}$$

The depth and discharge profiles change rapidly with time. The profiles of Ritter are the solid lines, while the numerical simulation results for the TDWs are the points in figure 2.

The local Froude number of the 1D solution according to (3.2) is

$$Fr_y = \frac{q_y}{\sqrt{gh^3}} = \frac{2(1+R)}{2-R} \quad \text{for } -1 < R < 2. \tag{3.3}$$

At the gate where $y = 0$ and $R = 0$, the flow is critical with $Fr_y = 1$. The depth and discharge of this critical flow are

$$h = h_{critical} = \tfrac{4}{9}H_o, \quad (q_y)_{critical} = \tfrac{8}{27}\sqrt{gH_o^3}. \tag{3.4a,b}$$

The discharge q_y is zero at the advancing front and the recessing edge. The maximum discharge occurs in the critical-flow section: $(q_y)_{max} = (q_y)_{critical}$. The dimensionless discharge coefficient corresponding to this flow rate through the critical section is

$$q^*_{Ritter} = \frac{(q_y)_{max}}{\sqrt{gH_o^3}} = \frac{8}{27} \simeq 0.296. \tag{3.5}$$

Water moves through the critical section as it depletes on one side, filling the volume on the other side of the wave.

3.2. *The discharge coefficient of the 2D TDWs*

The discharge coefficients of the 2D TDWs as shown in figure 3 are comparable in magnitude with the 1D coefficient of Ritter. The flow through the gate opening is the integral of q_y over the length of the opening, $Q(t,\, Fr_o) = \int_o^L q_y(x,\, 0,\, t)\mathrm{d}x$. The corresponding discharge coefficient is $Q^*(t,\, Fr_o) = Q/(L\sqrt{gH_o^3})$. Immediately

https://doi.org/10.1017/jfm.2014.562 Published online by Cambridge University Press

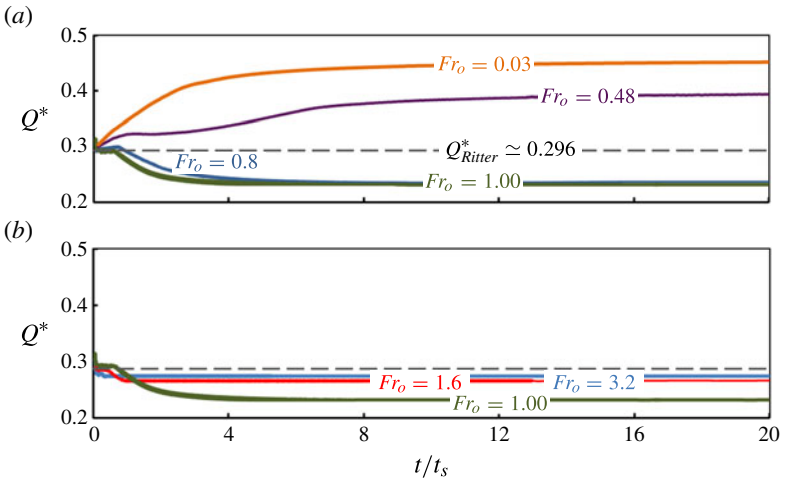


FIGURE 3. The discharge coefficient, $Q^*(t, Fr_o)$, and its dependence on the time t/t_s and on the main-flow Froude number Fr_o: (*a*) subcritical main flow with $Fr_o < 1$; (*b*) supercritical main flow with $Fr_o > 1$. The flow is considered to have reached steady state at time $t = 10t_s$ as the total flow rate Q^* has closely approached its asymptote at this time.

after the opening of the gate, all discharge coefficients are equal to the 1D value $q^*_{Ritter} \simeq 0.296$. The discharge coefficient increases with time for $Fr_o < 0.63$ and decreases with time for $Fr_o > 0.63$. Steady state is reached within a very short period of time, particularly for supercritical main flow. For subcritical main flow ($Fr_o < 1$), the discharge coefficient decreases as the main-flow Froude number, Fr_o, increases from 0 to approximately 0.9. For supercritical main flow ($Fr_o \geqslant 1$), on the other hand, the discharge coefficient increases with the Fr_o.

4. TDWs on a flat bed in steady state

Figure 4 shows the flow patterns of the TDWs on a flat bed in the steady state. The patterns delineated by the local Froude number $Fr = \sqrt{\boldsymbol{u}^2 + \boldsymbol{v}^2}/\sqrt{gh}$ on the x–y plane are obtained at a time $t = 10\,t_s$. The flow is considered to have reached the steady state as the total outflow rate Q has nearly reached its asymptote at this time, as shown in figure 3. There are two distinctively different steady-state flow patterns. Figures 4(*a–c*) are the patterns for subcritical main flow with $Fr_o = 0.03$, 0.48 and 0.80, and figure 4(*d*) for supercritical main flow with $Fr_o = 1.28$. For subcritical main flow with $Fr_o < 1$, a supercritical expansion on the upstream side is followed by subcritical outflow. Rapid change in depth and velocity occurs across the hydraulic jump as the flow changes from supercritical to subcritical flow. The length L_{super} defines the location of the hydraulic jump at the gate, as shown in figure 1. Figure 5 shows the fraction of supercritical outflow, L_{super}/L. The supercritical fraction of the flow increases in length linearly with the main-flow Froude number Fr_o in the range varying from $Fr_o = 0$ to 1. The entire outflow becomes supercritical when $Fr_o \geqslant 1$.

4.1. *Prandtl–Meyer expansion for TDWs with* $Fr_o > 1$

In the steady state, the diversion of the supercritical outflow on a flat bed is the Prandtl–Meyer expansion. Mizumura *et al.* (2003) provided the following explicit

https://doi.org/10.1017/jfm.2014.562 Published online by Cambridge University Press

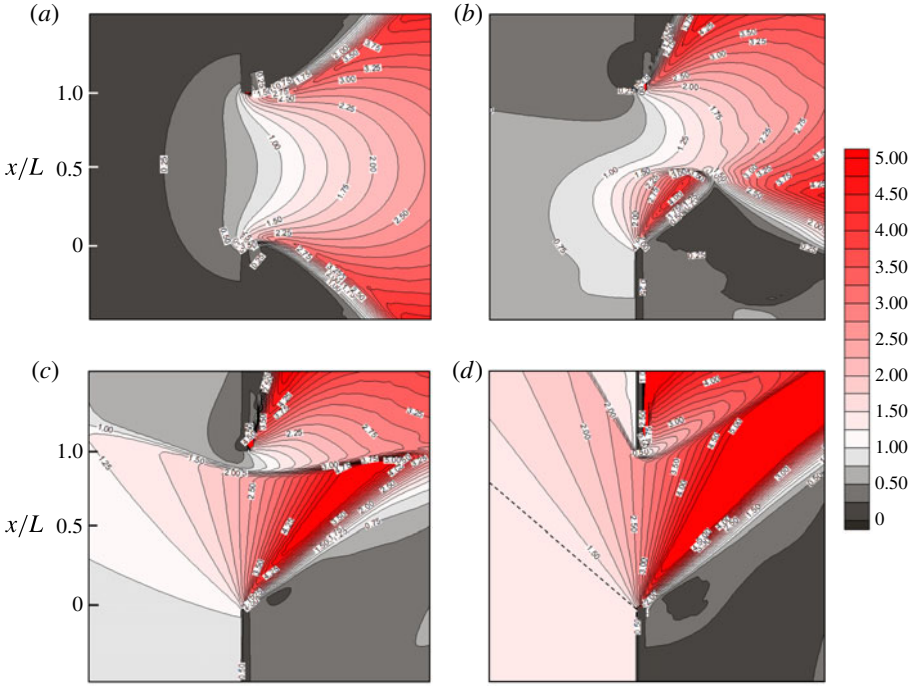


FIGURE 4. The TDWs on a flat bed at the steady state when time $t = 10t_s$. The main-flow Froude numbers are (*a*) $Fr_o = 0.03$, (*b*) $Fr_o = 0.48$, (*c*) $Fr_o = 0.80$ and (*d*) $Fr_o = 1.28$. The contour values are the local Froude numbers. The dashed line in (*d*) indicates the 'Froude line' between the undisturbed main flow and the diversion expansion fan.

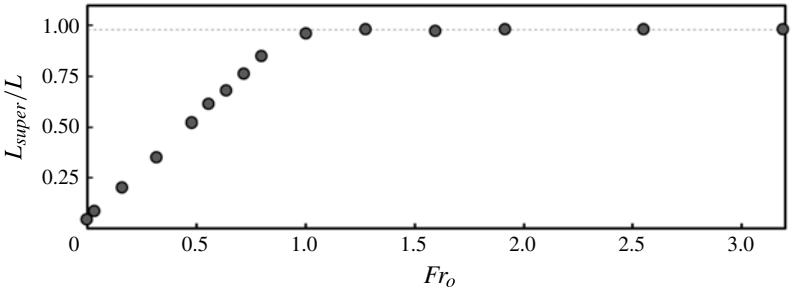


FIGURE 5. The length fraction L_{super}/L of the supercritical flow expansion.

expressions for the velocity components $(\boldsymbol{v}_r, \boldsymbol{v}_\theta)$ and the depth h of the Prandtl–Meyer expansion in plane polar coordinates (r, θ):

$$\boldsymbol{v}_r = \sqrt{2gE}\sin\left(\frac{\theta+\theta_1}{\sqrt{3}}\right), \quad \boldsymbol{v}_\theta = \sqrt{\frac{2gE}{3}}\cos\left(\frac{\theta+\theta_1}{\sqrt{3}}\right), \quad h = \frac{2E}{3}\cos^2\left(\frac{\theta+\theta_1}{\sqrt{3}}\right). \tag{4.1a–c}$$

The angle θ is clockwise from the opening where $y = 0$. These solutions give $Fr_\theta = \boldsymbol{v}_\theta/\sqrt{gh} = 1$ throughout the expansion fan and a critical outflow of $Fr_y = \boldsymbol{v}/\sqrt{gh} = 1$

https://doi.org/10.1017/jfm.2014.562 Published online by Cambridge University Press

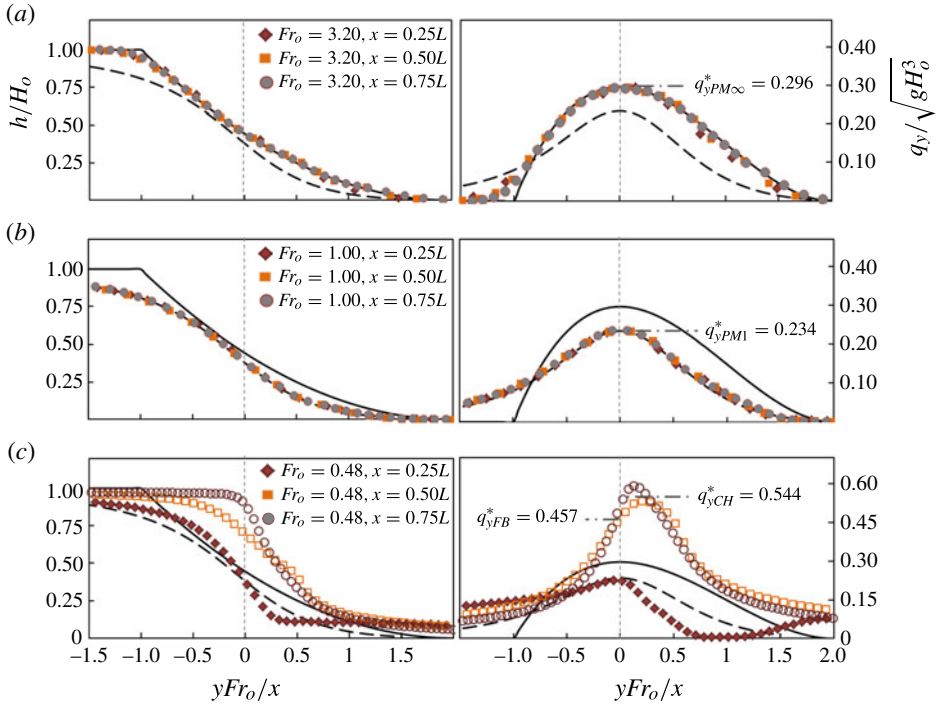


FIGURE 6. Depth h-profile (left) and lateral discharge q_y-profile (right) of the TDWs in the steady state for (*a*) $Fr_o = 3.2$, (*b*) $Fr_o = 1.0$ and (*c*) $Fr_o = 0.48$. The dashed and the solid lines are the Prandtl–Meyer profiles for the limiting cases of $Fr_o = 1$ and $Fr_o \to \infty$, respectively.

at the opening where $y = 0$. The corresponding flow rate in the y direction is

$$q_y = [\boldsymbol{v}_r \sin\theta + \boldsymbol{v}_\theta \cos\theta]\, h. \tag{4.2}$$

The specific energy E and the angle θ_1 in (4.1) are

$$E = H_o \left[\frac{1}{2}Fr_o^2 + 1\right], \quad \theta_1 = \sqrt{3}\cos^{-1}\sqrt{\frac{3}{2+Fr_o^2}} + \sin^{-1}\frac{1}{Fr_o}, \tag{4.3a,b}$$

which are evaluated at the 'Froude line' between the expansion fan and the undisturbed main flow where $\theta = -\sin^{-1}[1/Fr_o]$. At the Froude line, $h = H_o$ and $\sqrt{\boldsymbol{v}_r^2 + \boldsymbol{v}_\theta^2} = U_o$.

4.2. *Prandtl–Meyer expansion in terms of Ritter's similarity variable*

For observation in a reference frame moving with the undisturbed main flow, the space and time are related through the Galilean transformation $x = U_o t$. With this transformation, $t\sqrt{gH_o} = x/Fr_o$, Ritter's similarity variable becomes $R = yFr_o/x$. The h- and q_y-profiles of the Prandtl–Meyer expansion given by (4.1) and (4.2) are unique functions of Ritter's similarity variable. The dashed and solid lines in figure 6 are respectively the limiting profiles when $Fr_o = 1$ and $Fr_o \to \infty$. The points in the figure

https://doi.org/10.1017/jfm.2014.562 Published online by Cambridge University Press

denote the numerical simulation results in three outflow sections, $x = 0.25L$, $0.5L$ and $0.75L$. For main-flow Froude numbers of $Fr_o = 3.2$ and 1.0, the points in figures 6(*a*,*b*) respectively fall between the solid line and the dashed line, supporting the use of Ritter's similarity variable to describe the Prandtl–Meyer expansion. Exactly like the 1D solution of Ritter, the outflow rate peaks in a critical-flow section where the local Froude number $Fr_y = (q_y)_{max}/\sqrt{gh^3} = 1$. The lateral flow through the gate opening is the exact value of Ritter, $q^*_{yPM\infty} = q^*_{Ritter} = (q_y)_{max}/\sqrt{gH_o^3} = 0.296$, as the main-flow Froude number $Fr_o \to \infty$. The rate drops to a value of $q^*_{yPM1} = 0.234$ as the main-flow Froude number approaches its lowest value of $Fr_o = 1$. The drop in the flow rate from $q^*_{yPM\infty}$ to q^*_{yPM1} is most likely due to the retreating wavefront velocity at the Froude line. A greater retreating velocity leads to a lower critical-flow rate. In the reference frame moving with the main flow, the retreating velocity is $\boldsymbol{v} \to -\infty$ at the Froude line if the main-flow Froude number is $Fr_o = 1$. The retreating velocity is reduced to the value of Ritter, $\boldsymbol{v} = -\sqrt{gH_o}$, as the main-flow Froude number $Fr_o \to \infty$.

4.3. *TDWs for subcritical main flow*

Figure 6(*c*) shows the simulation profiles for the subcritical main flow of $Fr_o = 0.48$. The solid symbols in the figure delineate the depth and discharge profiles in the expansion fan upstream of the jump. They are comparable with the Prandtl–Meyer profiles for $Fr_o = 1$ defined by the dashed lines, with a peak discharge of $q^*_y \simeq q^*_{yPM1} = 0.234$. However, the profiles defined by the open symbols for the pool of water downstream of the hydraulic jump are very different. The peak discharge in the pool is significantly higher. The flow downstream of the hydraulic jump (where $q_x \ll q_y$) is nearly unaffected by the main flow. Therefore, the outflow from the pool can be roughly characterized by the head H_o, leading to a peak discharge of $q_y = \sqrt{g(2H_o/3)^3}$ and a peak discharge coefficient of $q^*_{yCH} = \sqrt{(\frac{2}{3})^3} = 0.544$. The peak occurs at the critical depth $h_c = 2H_o/3$ where the Froude number $\boldsymbol{v}/\sqrt{gH_o} = 1$. The depth at the opening downstream of the hydraulic jump is slightly greater than the critical depth; therefore, the discharge coefficient $q^*_{yFB} \simeq 0.457$ at the opening is lower than the peak values.

5. Discharge coefficient over weirs and a flat bed

The simulation results thus far have been presented for the TDWs on a flat bed. A number of additional simulations have been carried out for the outflow over weirs. The results are compared with laboratory experimental observations. Some of the laboratory experiments were conducted for outflow on a flat bed. Most of the experiments were over sharp-crested weirs. Figure 7 shows all simulation results on the flat bed and over the weirs, and available experimental data for the total discharge coefficient $Q^* = [\int_0^L q_y \mathrm{d}x]/L\sqrt{gH_o^3}$.

5.1. *Discharge coefficient for diversion over a weir*

For the simulation over a weir, the bottom elevation is $z_o = \frac{1}{2}H_w[\cos(\pi y/W_w) + 1]$, gradually varying over the width of the weir from $y = -\frac{1}{2}W_w$ to $y = \frac{1}{2}W_w$. With the weir, the depth H in the main flow is not uniform. However, the main-flow Froude number $Fr_o = U/\sqrt{gH}$ is unchanged by varying the velocity U across the main flow. The width-to-height ratio of the weir, W_w/H_w, is a parameter of the

https://doi.org/10.1017/jfm.2014.562 Published online by Cambridge University Press

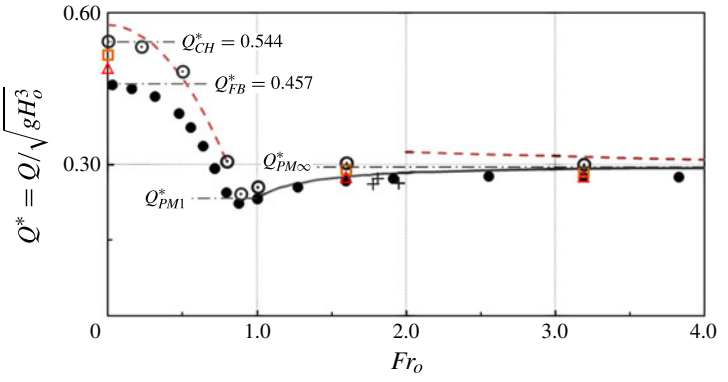


FIGURE 7. Dependence of the steady-state discharge coefficient on the main-flow Froude number. The solid symbols denote the discharge coefficient obtained from the simulations over a flat bed. The open symbols △, □ and ⊙ denote the simulated outflow over weirs of $W_w/H_w = 16$, 8 and 4, respectively. The solid line is the Prandtl–Meyer solution for the expansion. The + symbol represents the laboratory data obtained by Mizumura *et al.* (2003). The red dashed lines are the empirical equations (5.1) and (5.2) derived from laboratory experiments over a sharp-crested weir by Subramanya & Awasthy (1972).

weir that affects the diversion flow rate, which increases with the steepness of the weir. For a main-flow Froude number of $Fr_o = 0$, the increases from the flat bed value are 7 %, 13 % and 19 % for ratios of $W_w/H_w = 16$, 8 and 4, respectively. For $Fr_o = 1.6$ the increases are 3 %, 8 %, 14 % and for $Fr_o = 3.2$ the increases are 0.3 %, 4 %, 8.9 %, respectively. The gradual rise in bottom elevation has only a small effect on the discharge coefficient. However, a more rapid rise in bottom elevation for the sharper-crested weir of $W_w/H_w = 4$ increases the discharge coefficient to $Q^*_{weir} = 0.545$, 0.307, 0.255, 0.304, 0.301 for $Fr_o = 0$, 0.8, 1.00, 1.6, 3.2, respectively. These coefficients are marked by the ⊙ symbol in figure 7.

For subcritical main flow ($Fr_o < 1$), the presence of the weir has the effect of bringing the critical-flow section closer to the crest of the weir. The result is an increase in the discharge coefficient. For zero main flow the increase is from $Q^*_{FB} = q^*_{yFB} = 0.457$ to a value of $Q^*_{CH} = q^*_{yCH} = 0.544$, as shown in figure 7. The derivation for the value of q^*_{yCH} has been previously given in § 4.3. Increasing the main-flow Froude number Fr_o from 0 to 1 progressively increases the presence of the supercritical flow expansion and reduces the contribution of the subcritical outflow downstream of the hydraulic jump. The consequence is a reduction of the discharge coefficient in the subcritical range of main-flow Froude number, as shown in figure 7.

The effect of the weir on the outflow in the supercritical range of main-flow Froude number ($Fr_o > 1$) is different. All outflows from the Prandtl–Meyer expansion are critical with $Fr_y = v/\sqrt{gh} = 1$ at the gate opening (see § 4.1). The presence of the weir does not change the location of the critical section. It does, however, produce a narrower expansion fan, and hence the tendency for supercritical main flow to increase the discharge coefficient toward the rate of Ritter, $Q^*_{PM\infty} = q^*_{yPM\infty} = 0.296$.

5.2. *Laboratory experimental investigation*

Mizumura *et al.* (2003) have measured the diversion flow rate in laboratory experiments over a flat bed. Their data are affected by the bed friction but are only

https://doi.org/10.1017/jfm.2014.562 Published online by Cambridge University Press

slightly below the discharge coefficient obtained from the simulations. Subramanya & Awasthy (1972) have conducted laboratory experiments to measure the diversion flow rate over a sharp-crested weir and on a flat bed. They introduced the discharge coefficient C_d via $Q = \frac{2}{3}C_d\sqrt{2gH_o^3}$, and proposed the following semi-empirical formulae to fit their data:

$$C_d = 0.611\sqrt{1-\left(\frac{3Fr_o^2}{Fr_o^2+2}\right)} \quad \text{for } Fr_o < 0.8, \tag{5.1}$$

$$C_d = 0.36 - 0.008\,Fr_o \quad \text{for } Fr_o > 2. \tag{5.2}$$

The dashed lines in figure 7 are these formulae evaluated for $Q^* = \frac{2}{3}\sqrt{2}C_d$. The ratios of the main-flow width to the side-weir length varying from $B/L = 5$ to 1 in the laboratory experiments of Subramanya & Awasthy (1972) are not the same as the width-to-length ratios in the simulations. The trend of the numerical simulation results is nevertheless consistent with the experimental data.

6. Conclusion

The diversion of water to the side of a main flow produces a family of TDWs that is dependent on the Froude number of the main flow. For subcritical main flow ($Fr_o < 1$), the TDWs are supercritical flow expansions followed by a hydraulic jump to subcritical outflows. For supercritical main flow ($Fr_o > 1$), the TDWs are expansions that approach rapidly the steady-state solution of Prandtl–Meyer. The simulations of flow over weirs have produced discharge coefficients that follow the trend of dependence on the main-flow Froude number in a manner that is consistent with the data obtained from laboratory observations. The agreement of the simulations with analytical solutions is validation of the present numerical method, showing that it can be relied on to find solutions to other related flow-diversion problems, including the problems studied by Vazquez *et al.* (2008), Ghostine *et al.* (2013) and others. The method can also be utilized to study the erosion of channels and deposition of sediments in situations where the bottom of the channel varies in space and in time.

References

Chu, V. H. & Gao, C. 2013 False diffusion produced by flux limiters. *Comput. Therm. Sci.* **5** (6), 503–520.

Ghostine, R., Vazquez, J., Terfous, A., Riviere, N., Ghenaim, A. & Mose, R. 2013 A comparative study of 1D and 2D approaches for simulating flows at right angled dividing junctions. *Appl. Maths Comput.* **219** (10), 5070–5082.

Hogg, A. J. & Pritchard, D. 2004 The effects of hydraulic resistance on dam-break and other shallow inertial flows. *J. Fluid Mech.* **501**, 179–212.

Liepmann, H. W. & Roshko, A. 2013 *Elements of Gasdynamics*. Courier Dover Publications.

Liggett, J. A. 1994 *Fluid Mechanics*. McGraw-Hill Higher Education.

Mahmodinia, S., Javan, M. & Eghbalzadeh, A. 2014 The flow field and free surface pattern of the submerged side weir with different lengths. *Arab. J. Sci. Eng.* **39** (6), 4461–4472.

Mizumura, K., Yamasaka, M. & Adachi, J. 2003 Side outflow from supercritical channel flow. *J. Hydraul. Engng* **129** (10), 769–776.

Pinilla, C. E., Bouhairie, S., Tan, L. W. & Chu, V. H. 2010 Minimal intervention to simulations of shallow-water equations. *J. Hydro-Environ. Res.* **3** (4), 201–207.

Ritter, A. 1892 Die Fortpflanzung der Wasserwellen. *Z. Verein. Deutsch. Ing.* **36** (33), 947–954.

Subramanya, K. & Awasthy, S. C. 1972 Spatially varied flow over side-weirs. *J. Hydraul. Div.* **98** (1), 1–10.

https://doi.org/10.1017/jfm.2014.562 Published online by Cambridge University Press

SWEBY, P. K. 1984 High resolution schemes using flux limiters for hyperbolic conservation laws. *SIAM J. Numer. Anal.* **21** (5), 995–1011.

VAZQUEZ, J., KESSERWANI, G. & RIVIERE, N. 2008 Use of side-weir models and shallow water equations with TVD scheme for open channel bifurcations. In *11th International Conference on Urban Drainage, Edinburgh, Scotland*.

https://doi.org/10.1017/jfm.2014.562 Published online by Cambridge University Press